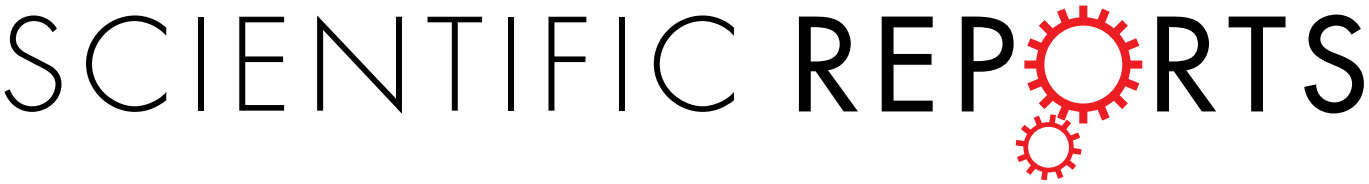

OPEN

Hybrid quantum gates between flying photon and diamond nitrogen-vacancy centers assisted by optical microcavities

Received: 12 February 2015
Accepted: 01 May 2015
Published: 14 August 2015

Hai-Rui Wei & Gui Lu Long

Hybrid quantum gates hold great promise for quantum information processing since they preserve the advantages of different quantum systems. Here we present compact quantum circuits to deterministically implement controlled-NOT, Toffoli, and Fredkin gates between a flying photon qubit and diamond nitrogen-vacancy (NV) centers assisted by microcavities. The target qubits of these universal quantum gates are encoded on the spins of the electrons associated with the diamond NV centers and they have long coherence time for storing information, and the control qubit is encoded on the polarizations of the flying photon and can be easily manipulated. Our quantum circuits are compact, economic, and simple. Moreover, they do not require additional qubits. The complexity of our schemes for universal three-qubit gates is much reduced, compared to the synthesis with two-qubit entangling gates. These schemes have high fidelities and efficiencies, and they are feasible in experiment.

A quantum computer[1] is more powerful than a classical computer in solving certain computationally demanding tasks. Quantum logic gates are the fundamental building blocks of a quantum computer, and a quantum computing task can be completed using a sequence of quantum gates as described in a quantum circuit. It is well known that any quantum computing can be decomposed into a sequence of single-qubit gates and two-qubit entangling gates[2], and analytical expressions[3] for an arbitrary n-qubit unitary gate have been explicitly derived using the methods provided in Ref. 2. One of the most popular universal quantum gates is the controlled-NOT (CNOT) gate. Quantum circuit received great attention over the years, in particular the CNOT gate (or the controlled phase gate)[2–10] and the hyperparallel CNOT gate[11–13]. The theoretical lower bound of an unstructured n-qubit quantum computation is $(4^n - 3n - 1)/4$ CNOT gates[5]. In multi-qubit systems, the fundamental three-qubit Toffoli gate[14] or Fredkin gate[15] form a family of universal quantum gates with the help of Hadamard operations, and they are valuable in fault-tolerant quantum circuits and some quantum algorithms. The realization of a Toffoli gate or a Fredkin gate in terms of two-qubit entangling gates is troublesome as the optimal cost is six CNOT gates[16] for a Toffoli gate and five two-qubit entangling gates for a Fredkin gate[17]. It is desirable to seek efficient schemes for directly implementing the Toffoli and Fredkin gates so as to speedup the quantum computation.

A single photon is a perfect information carrier and it has a flexible controllability. However, it seems unsuitable for quantum computing as the direct interaction between individual photons is very weak. Different to photonic qubit[18,19], matter qubits, such as atoms, quantum dots (QDs), superconduction junctions, and diamond nitrogen-vacancy (NV) defect centers, are widely utilized in quantum computing because of their long-lived coherence time and their good scalability. Compared with other candidates, a diamond NV center is a particularly promising one for a qubit as it has an ultralong coherence time

State Key Laboratory of Low-Dimensional Quantum Physics and Department of Physics, Tsinghua University, Beijing 100084, China. Correspondence and requests for materials should be addressed to G.L.L. (email: gllong@tsinghua.edu.cn)

(1.8 ms)[20] even at the room temperature. In a diamond NV center, the electron spin can be exactly populated by the optical pumping with 532 nm light[21], and it can be manipulated[21–24] and readout[25,26] by using the microwave excitation. The techniques to transfer the information from electron spins to nuclear spins were developed well[27–29]. Besides, some important tasks in quantum computation have been investigated and even been realized in experiment on diamond NV centers. For example, in 2004, Jelezko *et al.*[30] carried out the experiments for implementing the hybrid controlled-ROT gate on an electron-nuclear system. In 2012, Sar *et al.*[31] realized the decoherence-protected conditional rotation gates on hybrid electron-nuclear systems. In 2010, Yang *et al.*[32] proposed a conditional phase gate on three diamond NV centers. In 2013, Wei and Deng[33] proposed some compact schemes for implementing universal gates on diamond NV centers, and Wang *et al.*[34] designed a quantum circuit for the photonic controlled phase gate via a diamond NV center. In 2015, Ren, Wang and Deng[13] presented the dipole induced transparency of a diamond NV center embedded in a photonic crystal cavity coupled to two waveguides, and proposed two universal hyperparallel hybrid photonic quantum logic gates, including a hybrid hyper-controlled-NOT gate and a hybrid hyper-Toffoli gate, on photon systems in both the polarization and the spatial-mode degrees of freedom, which can be used to perform more quantum operations with less resources and depress the resources consumed and the photonic dissipation. Recently, some interesting works for quantum information processing have been achieved on diamond NV centers, such as entanglement generation[35–41], quantum manipulation[42–44], quantum teleportation between solid-state qubits separated by three meters[45], and hyperentanglement[46] and entanglement[47,48] purification and concentration.

A light-matter system[49–52] coupled to a cavity provides an important platform to study quantum information processing. For example, some important schemes for the conventional parallel quantum computation[52–55] or the hyperparallel photonic quantum computation[11–13] were proposed with the light-matter platform coupled to optical microcavities. By using a flying photon as a bus, schemes for universal gates on atoms[56] and QDs[57] have been proposed. Hybrid quantum gates on two or more physical systems inherit all the advantages of the different systems.

In this paper, we focus on designing compact quantum circuits to implement CNOT, Toffoli, and Fredkin gates between a flying photon and solid-state diamond NV centers coupled to cavities. These quantum circuits are constructed by utilizing the input-output process of the single photon as a result of cavity quantum electrodynamics and optical spin selection rules. The schemes well work at the degeneracy of the spin 1 system and the gate's mechanism is deterministic in principle. The target qubits are encoded on the ground states of the electrons $|m_s = \pm 1\rangle$ associated with the diamond NV centers. The control qubit is encoded on the polarizations of the flying single photon. Our schemes have some advantages. First, our quantum circuits for these universal quantum gates are compact and economic. Second, they do not require additional qubits. Third, the control qubit is the flying photon which has the flexible controllability. Fourth, the target qubits are encoded on the spins of the electrons associated with NV centers which have the relatively long coherence time even at room temperature and are perfect for the storage of quantum information. Fifth, the complexity of our schemes for three-qubit quantum gates beats their synthesis procedures largely. The high fidelities and efficiencies of our schemes show that they may be feasible with current technology.

Results

A diamond nitrogen-vacancy center confined in an optical resonant microcavity. A diamond NV center consists of a vacancy adjacent to a substitutional nitrogen atom (typically ^{14}N). In a diamond NV center, both the nuclear spins (typically ^{13}C with $I = 1/2$ or ^{14}N with $I = 1$) and the electron spins are promising for quantum information processing. The ground states of the electron, $|0\rangle \equiv |m_s = 0\rangle$ and the two-fold degenerate states $|\pm\rangle \equiv |m_s = \pm 1\rangle$, is split by $D \approx 2.87$ GHz in a zero external field due to the spin-spin interaction[58]. The six excited states[39] $|A_1\rangle = (|E_-\rangle|+\rangle - |E_+\rangle|-\rangle)/\sqrt{2}$, $|A_2\rangle = (|E_-\rangle|+\rangle + |E_+\rangle|-\rangle)/\sqrt{2}$, $|E_x\rangle = |X\rangle|0\rangle$, $|E_y\rangle = |Y\rangle|0\rangle$, $|E_1\rangle = (|E_-\rangle|-\rangle - |E_+\rangle|+\rangle)/\sqrt{2}$, and $|E_2\rangle = (|E_-\rangle|-\rangle + |E_+\rangle|+\rangle)/\sqrt{2}$ are dominated by the NV center's C_{3v} symmetry and the spin-spin, spin-orbit interactions without external strain and electric or magnetic fields. Here $|E_\pm\rangle$, $|X\rangle$, and $|Y\rangle$ are the orbital states of an NV center. The spin-orbit interaction (5.5 GHz)[59,60] splits the excited states into three two-fold degeneracy pairs (A_1, A_2) (to be shifted up), (E_x, E_y), and (E_1, E_2) (to be shifted down). The spin-spin interaction (1.42 GHz) shifts up states (A_1, A_2, E_1, and E_2) by 1.42/3 GHz and shifts down states (E_x, E_y) by $2 * 1.42/3$ GHz[59,60]. Besides, it splits A_2 and A_1 by ± 1.55 GHz[59,60]. The local non-axial high strain (10 GHz, larger than the spin-orbit splitting in the presence of the zero field) splits the excited states into two branches, (A_2, A_1, and E_x) and (E_y, E_1, and E_2). The state $|A_2\rangle$ is robust against the relatively small strain and magnetic fields with the stable symmetry properties, preserving the polarization properties of its optical transitions. The frequency of the spin-selective optical resonant transition can be tuned via an application of a controlled external electric field[60–64]. In 2011, Bassett *et al.*[64] experimentally demonstrated an exceeding 10 GHz optical transition frequency. The transitions between the ground states are in the microwave frequency regime, and the transitions between the ground states and the excited states are in the optical regime. With microwave and laser, one can prepare, store, and read out the states of the solid-state electron spins[65]. Here we encode the qubit on the sublevels $|\pm\rangle$, and take

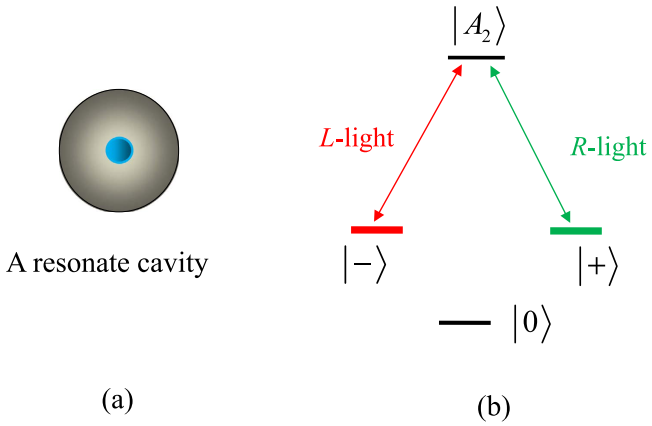

Figure 1. (**a**) Schematic diagram of an NV-cavity system. (**b**) The energy-level diagram of an NV-cavity system. The triple ground states $|\pm\rangle \equiv |m_s = \pm 1\rangle$ are chosen to act as the two levels for an electron-spin qubit. The excited state $|A_2\rangle = (|E_-\rangle|+1\rangle + |E_+\rangle|-1\rangle)/\sqrt{2}$ is an auxiliary state. $|\pm\rangle \rightarrow |A_2\rangle$ are driven by the right- and left- circularly-polarized photons, respectively.

$|A_2\rangle$ as an auxiliary state. $|A_2\rangle$ decays into $|\pm\rangle$ with the right-circularly-polarized (R) and left-circularly-polarized (L) photons [see Fig. 1b], respectively, owning to total angular momentum conservation. They take place with the equal probability.

In 2011, Chen *et al.*[41] discussed a composite unit, that is, a diamond NV center confined inside a single-sided resonator [see Fig. 1a]. Combing the Heisenberg equations of motion[66]

$$\begin{aligned}\frac{d\hat{a}}{dt} &= -\left[i(\omega_c - \omega_p) + \frac{\kappa}{2}\right]\hat{a}(t) - g\sigma_-(t) - \sqrt{\kappa}\,\hat{a}_{in},\\ \frac{d\sigma_-}{dt} &= -\left[i(\omega_0 - \omega_p) + \frac{\gamma}{2}\right]\sigma_-(t) - g\sigma_z(t)\hat{a}(t) + \sqrt{\gamma}\,\sigma_z(t)\hat{b}_{in}(t),\end{aligned} \tag{1}$$

and the standard input-output relation for the cavity

$$\hat{a}_{out} = \hat{a}_{in} + \sqrt{\kappa}\,\hat{a}(t), \tag{2}$$

the explicit expression of the reflection coefficient for the NV-cavity unit in the weak excitation limit $\langle\sigma_z\rangle = -1$ can be written as[41,67]

$$r(\omega_p) = \frac{\left[i(\omega_c - \omega_p) - \frac{\kappa}{2}\right]\left[i(\omega_0 - \omega_p) + \frac{\gamma}{2}\right] + g^2}{\left[i(\omega_c - \omega_p) + \frac{\kappa}{2}\right]\left[i(\omega_0 - \omega_p) + \frac{\gamma}{2}\right] + g^2}. \tag{3}$$

Here $\hat{a}$ and σ_- are the annihilation operator of the cavity mode and the transition operator of the diamond NV center with the frequencies ω_c and ω_0, respectively. ω_p is the frequency of the input single photon. $\sigma_z(t)$ presents the inversion operator of the NV center. γ and κ are the NV decay rate and the cavity damping rate, respectively. g is the coupling strength between an NV center and a cavity. The vacuum input field $b_{in}(t)$ has the commutation relation $[\hat{b}_{in}(t), \hat{b}^{\dagger}_{in}(t')] = \delta(t - t')$.

When the diamond NV center confined inside a resonant cavity interacts with a resonant single photon, i.e., $\omega_0 = \omega_c = \omega_p$, the reflection coefficients for the hot cavity ($g \neq 0$) and the cold cavity ($g = 0$) can be written as

$$r = \frac{-\kappa\gamma + 4g^2}{\kappa\gamma + 4g^2}, \quad r_0 = -1. \tag{4}$$

That is, the change of the incident photon can be summarized as follows[41]:

$$\begin{aligned}|R\rangle|+\rangle &\xrightarrow{NV} |r||R\rangle|+\rangle, \qquad |L\rangle|-\rangle \xrightarrow{NV} |r||L\rangle|-\rangle,\\ |R\rangle|-\rangle &\xrightarrow{NV} -|R\rangle|-\rangle, \qquad |L\rangle|+\rangle \xrightarrow{NV} -|L\rangle|+\rangle.\end{aligned} \tag{5}$$

When $g \geq 5\sqrt{\gamma\kappa}$ and $\omega_0 = \omega_c = \omega_p$, $r(\omega_p) \simeq 1$ and $r_0(\omega_p) = -1$[41], and Eq. (5) becomes

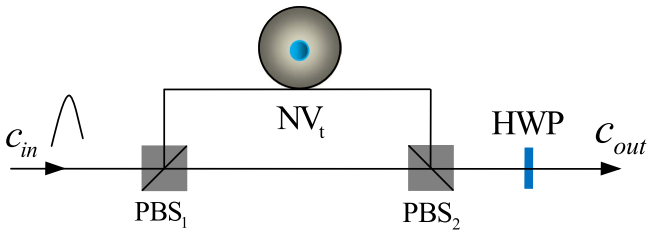

Figure 2. Compact quantum circuit for implementing the CNOT gate on a hybrid photon-NV system with the flying single photon polarization as the control qubit and the electron spin in the diamond NV center as the target qubit. PBS$_i$ ($i = 1, 2$) represents a polarizing beam splitter (PBS) which transmits the R-polarized photon and reflects the L-polarized photon, respectively. HWP represents a half-wave plate oriented at 0° and it is used to complete the unitary transformation $\sigma_z = |R\rangle\langle R| - |L\rangle\langle L|$ on a photon.

$$\begin{aligned} |R\rangle|+\rangle &\xrightarrow{\text{NV}} |R\rangle|+\rangle, \qquad |L\rangle|-\rangle \xrightarrow{\text{NV}} |L\rangle|-\rangle, \\ |R\rangle|-\rangle &\xrightarrow{\text{NV}} -|R\rangle|-\rangle, \qquad |L\rangle|+\rangle \xrightarrow{\text{NV}} -|L\rangle|+\rangle. \end{aligned} \tag{6}$$

Compact quantum circuit for implementing a hybrid CNOT gate. The framework of our proposal for implementing a CNOT gate is shown in Fig. 2. It performs a not operation on the diamond NV center when the flying single photon is in state $|L\rangle$. Let us describe its principle in detail as follows.

Suppose that the input state of the composite system composed of the flying single photon and the diamond NV center is

$$|\psi_{\text{in}}\rangle = \left(\cos\ \alpha|R\rangle_c + \sin\ \alpha|L\rangle_c\right) \otimes \left(\cos\ \beta|+\rangle_t + \sin\ \beta|-\rangle_t\right). \tag{7}$$

Here subscripts c and t represent the control qubit (the flying single photon) and the target qubit (the diamond NV center), respectively. First, the input single photon is split into two wave-packets by a polarizing beam splitter (PBS), say PBS$_1$. Second, the R-polarized component does not interact with the diamond NV center, whereas the L-polarized component interacts with the diamond NV center and then arrives at PBS$_2$ simultaneously with the R-polarized component. Third, before and after the photon interacts with the diamond NV center, a Hadamard operation H_e is performed on the diamond NV center, respectively. Here H_e completes the following transformations

$$|+\rangle \xrightarrow{H_e} |\rightarrow\rangle \equiv \frac{1}{\sqrt{2}}(|+\rangle + |-\rangle), \quad |-\rangle \xrightarrow{H_e} |\leftarrow\rangle \equiv \frac{1}{\sqrt{2}}(|+\rangle - |-\rangle). \tag{8}$$

Finally, a single-qubit operation $\sigma_z = |R\rangle\langle R| - |L\rangle\langle L|$ is performed on the output photon with a half-wave plate HWP oriented at 0°. With these operations, the state of the composite system evolves as follows:

$$\begin{aligned} |\psi_{\text{in}}\rangle &\xrightarrow{H_e,\ \text{PBS}_1} \left(\cos\ \alpha|R\rangle_c + \sin\ \alpha|L\rangle_c\right)\left(\cos\ \beta|\rightarrow\rangle_t + \sin\ \beta|\leftarrow\rangle_t\right) \\ &\xrightarrow{\text{NV}} \cos\ \alpha|R\rangle_c\left(\cos\ \beta|\rightarrow\rangle_t + \sin\beta|\leftarrow\rangle_t\right) - \sin\ \alpha|L\rangle_c\left(\cos\ \beta|\leftarrow\rangle_t + \sin\ \beta|\rightarrow\rangle_t\right) \\ &\xrightarrow{H_e,\ \text{PBS}_2} \cos\ \alpha|R\rangle_c\left(\cos\ \beta|+\rangle_t + \sin\ \beta|-\rangle_t\right) - \sin\ \alpha|L\rangle_c\left(\cos\ \beta|-\rangle_t + \sin\ \beta|+\rangle_t\right) \\ &\xrightarrow{\text{HWP}} |\psi_{\text{out}}\rangle = \cos\ \alpha|R\rangle_c\left(\cos\ \beta|+\rangle_t + \sin\ \beta|-\rangle_t\right) \\ &\qquad + \sin\ \alpha|L\rangle_c\left(\cos\ \beta|-\rangle_t + \sin\ \beta|+\rangle_t\right). \end{aligned} \tag{9}$$

The quantum circuit shown in Fig. 2 completes the transformation $|\psi_{\text{in}}\rangle \xrightarrow{\text{CNOT}} |\psi_{\text{out}}\rangle$. That is, it implements a CNOT gate on a hybrid photon-NV system. If the flying single photon is in state $|L\rangle$, the spins of the electron associated with the diamond NV center are flipped; otherwise, the spins of the electron remain unchanged.

Compact quantum circuit for implementing a Toffoli gate on a hybrid system. The principle of our hybrid Toffoli gate is shown in Fig. 3. This gate performs a CNOT operation on the two diamond NV centers, NV$_{c_2}$ and NV$_t$, when the flying single photon c_1 is in state $|L\rangle$. Suppose that the system composed of c_1, NV$_{c_2}$, and NV$_t$ is prepared in the state

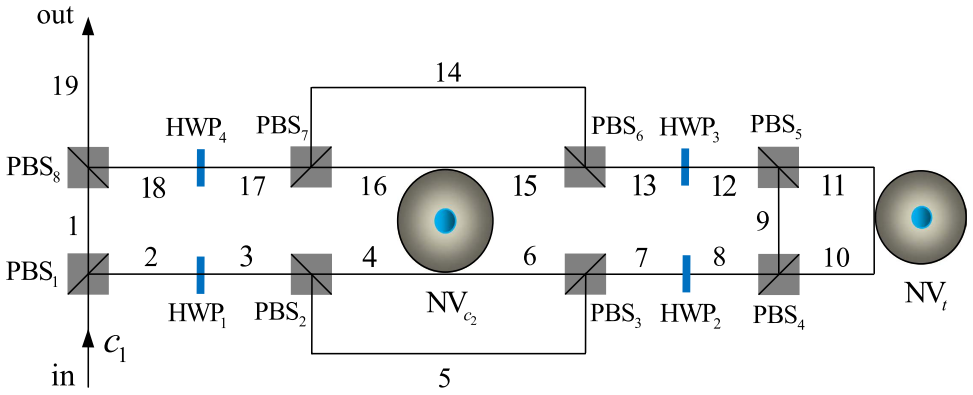

Figure 3. Compact quantum circuit for implementing a Toffoli gate which performs a CNOT operation on the two diamond NV centers if the flying single photon is in state $|L\rangle$.

$$|\Phi_{\text{in}}\rangle = \left(\cos\ \alpha|R\rangle_{c_1} + \sin\ \alpha|L\rangle_{c_1}\right) \otimes \left(\cos\ \beta|+\rangle_{c_2} + \sin\ \beta|-\rangle_{c_2}\right) \otimes \left(\cos\ \delta|+\rangle_t + \sin\ \delta|-\rangle_t\right). \tag{10}$$

Our hybrid Toffoli gate works with the following steps.

First, the R-polarized component of the input single photon c_1 is transmitted to spatial mode 1 by PBS_1 and then arrives at PBS_8 directly, whereas the L-polarized component is reflected to spatial mode 2 for interacting with the diamond NV centers. When the photon emits from spatial mode 2, it passes through the block composed of PBS_2, NV_{c_2}, and PBS_3, and a Hadamard operation H_p is performed on it with a half-wave plate (HWP) oriented at 22.5° before and after it passes through the block, respectively. We can obtain the following transformation induced by the above operations $\left(\text{PBS}_1 \rightarrow \text{HWP}_1 \rightarrow \text{PBS}_2 \rightarrow \text{NV}_{c_2} \rightarrow \text{PBS}_3 \rightarrow \text{HWP}_2\right)$

$$|\Phi_{\text{in}}\rangle \rightarrow |\Phi\rangle_1 = \Big[\cos\ \alpha|R_1\rangle_{c_1}(\cos\ \beta|+\rangle_{c_2} + \sin\ \beta|-\rangle_{c_2}) + \sin\ \alpha(\cos\ \beta|L_8\rangle_{c_1}|+\rangle_{c_2} - \sin\ \beta|R_8\rangle_{c_1}|-\rangle_{c_2})\Big]\left(\cos\ \delta|+\rangle_t + \sin\ \delta|-\rangle_t\right). \tag{11}$$

Here and below, we use $|R_i\rangle$ ($|L_i\rangle$) denotes the $R-$ ($L-$) polarized photon emitted from spatial mode i ($i = 1, 2, \ldots, 19$).

Second, the photon passes through the block composed of PBS_4, NV_t, and PBS_5, and before and after the photon interacts with NV_t, an H_e is performed on NV_t, respectively. These operations ($H_e \rightarrow \text{PBS}_4 \rightarrow \text{NV}_t \rightarrow \text{PBS}_5 \rightarrow H_e$) transform $|\Phi\rangle_1$ into $|\Phi\rangle_2$. Here

$$|\Phi\rangle_2 = \Big[\cos\alpha|R_1\rangle_{c_1}\left(\cos\beta|+\rangle_{c_2} + \sin\beta|-\rangle_{c_2}\right) + \sin\alpha\ \cos\beta|L_{12}\rangle_{c_1}|+\rangle_{c_2}\Big] \times \left(\cos\delta|+\rangle_t + \sin\delta|-\rangle_t\right) - \sin\alpha\ \sin\beta|R_{12}\rangle_{c_1} |-\rangle_{c_2}\left(\cos\delta|-\rangle_t + \sin\delta|+\rangle_t\right). \tag{12}$$

Third, the photon emitting from spatial mode 12 passes through the block composed of PBS_6, NV_{c_2}, and PBS_7. Before and after the photon passes through the block, an H_p is performed on it with HWP_3 and HWP_4, respectively. After the wave-packet emitting from spatial mode 18 arrives at PBS_8 simultaneously with the wave-packet emitting from spatial mode 1, the state of the system becomes

$$|\Phi_{\text{out}}\rangle = \Big[\cos\ \alpha|R_{19}\rangle_{c_1}\left(\cos\ \beta|+\rangle_{c_2} + \sin\ \beta|-\rangle_{c_2}\right) + \sin\ \alpha\ \cos\ \beta|L_{19}\rangle_{c_1}|+\rangle_{c_2}\Big] \times \left(\cos\ \delta|+\rangle_t + \sin\ \delta|-\rangle_t\right) + \sin\ \alpha\ \sin\ \beta|L_{19}\rangle_{c_1} |-\rangle_{c_2}\left(\cos\ \delta|-\rangle_t + \sin\ \delta|+\rangle_t\right). \tag{13}$$

From Eqs (10)–(13), one can see that the quantum circuit in Fig. 3 completes the transformation $|\Phi_{\text{in}}\rangle \xrightarrow{\text{controlled}-\text{CNOT}} |\Phi_{\text{out}}\rangle$. That is, it implements a Toffoli gate (it is also named a controlled-CNOT gate)

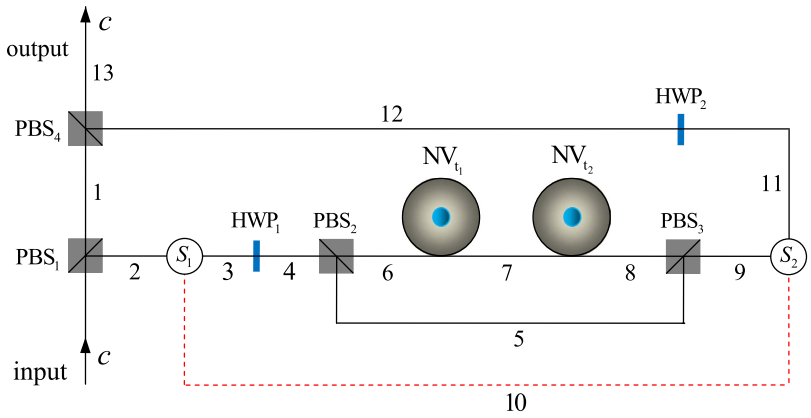

Figure 4. Quantum circuit for implementing a hybrid Fredkin gate with a flying single photon as the control qubit and the two diamond NV centers as the target qubits.

which performs a CNOT operation on the two diamond NV centers when the control photon is in state $|L\rangle$; otherwise, the states of the two NV centers keep unchanged.

Quantum circuit for implementing a deterministic Fredkin gate on a hybrid system. Our Fredkin gate is used to exchange the states of the two target diamond-NV-center-spin qubits, NV_{t_1} and NV_{t_2}, when the flying single photon c is in state $|L\rangle$; otherwise, the states of the two target qubits remain unchanged. The quantum circuit for implementing our Fredkin gate is shown in Fig. 4 and its principle can be explained as follows.

Let us consider an input state of the three-qubit hybrid system composed of the control photon c and the two target diamond NV centers NV_{t_1} and NV_{t_2},

$$|\Xi_{in}\rangle = (\cos\alpha|R\rangle_c + \sin\alpha|L\rangle_c) \otimes (\cos\beta|+\rangle_{t_1} + \sin\beta|-\rangle_{t_1}) \otimes (\cos\delta|+\rangle_{t_2} + \sin\delta|-\rangle_{t_2}). \quad (14)$$

When the injecting control photon c arrives at PBS_1, the state of the hybrid system is transformed from $|\Xi_{in}\rangle$ to $|\Xi_1\rangle$. Here

$$|\Xi_1\rangle = (\cos\alpha|R_1\rangle_c + \sin\alpha|L_2\rangle_c)(\cos\beta|+\rangle_{t_1} + \sin\beta|-\rangle_{t_1})(\cos\delta|+\rangle_{t_2} + \sin\delta|-\rangle_{t_2}). \quad (15)$$

The wave-packet emitting from spatial mode 1 arrives at PBS_4 directly and the optical switch S_1 leads the wave-packet emitting from spatial mode 2 to spatial mode 3. After an H_p is performed on the photon with HWP_1, it first passes through the block composed of PBS_2, NV_{t_1}, NV_{t_2}, and PBS_3, and then arrives at S_2. S_2 leads the photon to spatial mode 10, followed with S_1 which leads the photon to spatial mode 3 for passing through HWP_1. These operations $\left(S_1 \rightarrow HWP_1 \rightarrow PBS_2 \rightarrow NV_{t_1} \rightarrow NV_{t_2} \rightarrow PBS_3 \rightarrow S_2 \rightarrow S_1 \rightarrow HWP_1\right)$ transform the state of the hybrid system into

$$\begin{aligned}|\Xi_2\rangle = {} & \cos\alpha|R_1\rangle_c\left(\cos\beta|+\rangle_{t_1} + \sin\beta|-\rangle_{t_1}\right)\left(\cos\delta|+\rangle_{t_2} + \sin\delta|-\rangle_{t_2}\right) \\ & + \sin\alpha\left(\cos\beta\cos\delta|L_4\rangle_c|+\rangle_{t_1}|+\rangle_{t_2} - \cos\beta\sin\delta|R_4\rangle_c|+\rangle_{t_1}|-\rangle_{t_2}\right. \\ & \left. - \sin\beta\cos\delta|R_4\rangle_c|-\rangle_{t_1}|+\rangle_{t_2} + \sin\beta\sin\delta|L_4\rangle_c|-\rangle_{t_1}|-\rangle_{t_2}\right). \end{aligned} \quad (16)$$

Before and after the second round, an H_e is performed on each of NV_{t_1} and NV_{t_2}. These operations $(H_{e_2}, H_{e_3} \rightarrow PBS_2 \rightarrow NV_{t_1} \rightarrow NV_{t_2} \rightarrow PBS_3 \rightarrow H_{e_2}, H_{e_3} \rightarrow S_2 \rightarrow S_1)$ transform $|\Xi_2\rangle$ into

$$\begin{aligned}|\Xi_3\rangle = {} & \cos\alpha|R_1\rangle_c\left(\cos\beta|+\rangle_{t_1} + \sin\beta|-\rangle_{t_1}\right)\left(\cos\delta|+\rangle_{t_2} + \sin\delta|-\rangle_{t_2}\right) \\ & + \sin\alpha\left(\cos\beta\cos\delta|L_3\rangle_c|+\rangle_{t_1}|+\rangle_{t_2} - \cos\beta\sin\delta|R_3\rangle_c|-\rangle_{t_1}|+\rangle_{t_2}\right. \\ & \left. - \sin\beta\cos\delta|R_3\rangle_c|+\rangle_{t_1}|-\rangle_{t_2} + \sin\beta\sin\delta|L_3\rangle_c|-\rangle_{t_1}|-\rangle_{t_2}\right). \end{aligned} \quad (17)$$

Next, the photon passes through HWP_1 and the block composed of PBS_2, NV_{t_1}, NV_{t_2}, and PBS_2 in succession, and then S_2 leads it to spatial mode 11, followed with an H_p (i.e., let it passes through HWP_2). Finally, the wave-packet emitting from spatial mode 12 arrives at PBS_4 simultaneously with the wave-packet emitting from spatial mode 1. That is, these operations $\left(HWP_1 \rightarrow PBS_2 \rightarrow NV_{t_1} \rightarrow NV_{t_2} \rightarrow PBS_3 \rightarrow S_2 \rightarrow HWP_2 \rightarrow PBS_4\right)$ transform $|\Xi_3\rangle$ into

$$\begin{aligned}|\Xi_{out}\rangle = & \cos\ \alpha|R_{13}\rangle_c\left(\cos\ \beta|+\rangle_{t_1} + \sin\ \beta|-\rangle_{t_1}\right)\left(\cos\ \delta|+\rangle_{t_2} + \sin\ \delta|-\rangle_{t_2}\right)\\ & + \sin\ \alpha|L_{13}\rangle_c\left(\cos\ \beta|+\rangle_{t_2} + \sin\ \beta|-\rangle_{t_2}\right)\left(\cos\ \delta|+\rangle_{t_1} + \sin\ \delta|-\rangle_{t_1}\right).\end{aligned} \tag{18}$$

Putting all the pieces together, one can see that the quantum circuit shown in Fig. 4 completes the transformation $|\Xi_{in}\rangle \xrightarrow{\text{Fredkin}} |\Xi_{out}\rangle$. That is, the quantum circuit shown in Fig. 4 implements a Fredkin gate which exchanges the spins of the two electrons associated with the diamond NV centers NV_{t_1} and NV_{t_2} when the flying single photon is in state $|L\rangle$; otherwise, the states of the two target qubits remain unchanged.

Discussion

By far, several groups have experimentally demonstrated the coupling between a diamond NV center and a microcavity, such as microspheres[68–71], microdisks[72], photonic crystals[73–75], microtoroidal resonators[76,77], and fiber-based microcavity[78]. It is a challenge to achieve the strong coupling between the NV and the cavity in experiments with current technology. Fortunately, the strong coupling between NV centers in diamond nanocrystals and a whispering gallery mode (WGM) in a silica microsphere has been achieved[68]. Larsson *et al.*[69] showed that it is possible to achieve the strong coupling between NV centers in a diamond nanopillar coupled to a WGM in a silica microsphere. In 2013, Teissier *et al.*[79] realized an exceeding 10 MHz coupling strength between an NV center and a diamond mechanical oscillator. In 2006, Park *et al.*[68] observed the strong coupling ($g/2\pi = 55$ MHz, $\gamma/2\pi = 25$ MHz, $\kappa/2\pi = 50$ MHz) in a diamond NV center coupled to a WGM in a silica microsphere. Barclay *et al.*[80] showed that the strong coupling with the parameters $[g, \kappa, \gamma_{tot}]/2\pi = [2.25, 0.16, 0.013]$ GHz is possible in an NV nanocavity. In 2009, Barclay *et al.*[72] showed that the parameters $[g, \kappa, \gamma, \gamma_{ZPL}]/2\pi = [0.30, 26, 0.013, 0.0004]$ GHz can be achieved in experiment for coupling the NV centers in single crystal diamond to an chip-based microcavity. Here γ_{ZPL} is the spontaneous emission rate of a diamond NV center into the zero phonon line (ZPL). For NV-microtoridal resonators, $|r(\omega_p)| \sim 1$ can be achieved when $g = 2\pi \times 500$ MHz with $\kappa = 2\pi \times 10$ GHz or $\kappa = 2\pi \times 1$ GHz[41].

Our schemes work for the degenerate cavity modes, and it can be achieved by employing microtoroidal resonators[76,77,81,82], H1 photonic crystals[83,84], micropillars[85–87], or fiber-based[78] cavities. Our schemes are deterministic in principle. Our schemes have high fidelities and efficiencies if the photon loss caused by the linear optics are not taken into account. Certainly, we should take the photon loss into account in the practical applications[18] as there are the cavity absorption and scattering, and the absorption from linear optical elements (such as the fibers, PBS, and HWP). Different to the protocol for generating entanglement between two NV centers[37], our gates cannot be heralded by the destructive detection of a single photon. Our schemes can be inferred by the successful instances in postselection in practical applications of our gates. For example, when our hybrid gate is used for quantum information transfer, the successful transfer of the information from the NV electron spin to the single photon polarization indicates the success of our CNOT gate. In principle, the photon loss can be reduced by improving experiment techniques and fabrication processing. The ZPL emission of an NV center is only 3%–4% of the total emission. In 2011, Barclay *et al.*[88] enhanced the ZPL emission of an NV center in a WGM nanocavity from ~3% to ~16%. Subsequently, they[76] enhanced the ZPL emission of an NV center coupled to a microresonator from 3/100 to 36/133. In 2012, Faraon *et al.*[89] enhanced the ZPL emission by a factor of ~70 in photonic crystal cavities.

Fluctuations in the frequency of the optical transition of NV centers, due to the fluctuation in the charge environment, is a hurdle for our schemes. This spectral diffusion in the nanocavity devices results in an overall line width which can be much larger than the NV transition line width (13–16 MHz). Therefore, as that done by Delft's group[37], we should first check the transition frequency of the NV centers before our schemes. Spectral diffusion can be reduced by active stabilization technique, preselection of the transition frequency technique, or combination of high temperature annealing and subsequent surface treatment technique[90–92]. The optical transition frequencies of the two NV centers in our schemes for Toffoli and Fredkin gates can be tuned into resonance with each other by applying an external electric field[61].

Our schemes work not only for the two-fold sublevels encoded for the electron-spin qubits but also for the non-degenerate spin sublevels lifted by a small external magnetic field. Dréau *et al.*[93] demonstrated that the excited states occur sublevels anticrossing when $B \approx 510$ G and the one for the ground states when $B \approx 1020$ G. The state A_2 is robust against a relatively small magnetic field. For the non-degenerate

one, if only the *R*-polarized photon matches the resonance transition, our schemes can implement the CNOT, Toffoli, and Fredkin gates only with a little modification on the quantum circuit in Fig. 2.

Compared with the parity-measurement approach in Refs. [94,95] and the one based on control path and merging gates[96], the auxiliary qubits are not required in our schemes, and the number of the nonlinear interactions required for our CNOT gate is fewer than that in Refs. [94–96]. The complexity of our Toffoli and Fredkin gates beat their synthesis procedures in terms of two-qubit entangling gates largely as the well known cost of the Toffoli and Fredkin gates[16,17,96] are six CNOT gates and five two-qubit entangling gates, respectively.

In summary, we have presented compact quantum circuits for the hybrid universal quantum gates assisted by the input-output process of a single photon. Our CNOT, Toffoli, and Fredkin gates work with the single-photon polarizations as the control qubits and the electron spins associated with the diamond NV centers as the target qubits. Our schemes take the advantages of the theoretical and experimental progress in the fast electron-spin manipulation, the long-lived electron-spin coherence time, and the flexible controllability of the single photon. All our schemes are compact, economic, and simple. They have high fidelities and efficiencies with current technology.

Methods

Average fidelities and efficiencies of the gates. We use the fidelity and the efficiency to characterize the performance of our universal quantum gates. In order to characterize the construction of these gates, we specify the evolutions of the hybrid systems from the initial sates $|\psi_{in}\rangle$ to the output states $|\psi_{out}\rangle$ in the ideal case. The fidelity of a quantum gate is defined as $F = |\langle\psi_{out}|\psi'_{out}\rangle|^2$, and it is the probability that the normalized output state of the whole system in the ideal case $|\psi_{out}\rangle$ overlaps with the realistic state $|\psi'_{out}\rangle$. Taking the CNOT gate as an example, in the ideal case (i.e., $r(\omega_p) \simeq 1$ and $r_0(\omega_p) = -1$), the normalized output state of our scheme is given by Eq. (9), that is,

$$|\psi_{out}\rangle_{CT} = \cos\alpha|R\rangle_c\left(\cos\beta|+\rangle_t + \sin\beta|-\rangle_t\right) + \sin\alpha|L\rangle_c\left(\cos\beta|-\rangle_t + \sin\beta|+\rangle_t\right). \quad (19)$$

By substituting Eq. (5) for Eq. (6) and combing the evolutions of the state for the CNOT gate, the non-normalized output state in the realistic case becomes

$$\begin{aligned}|\psi'_{out}\rangle_{CT} = {} & \cos\alpha|R\rangle_c\left(\cos\beta|+\rangle_t + \sin\beta|-\rangle_t\right)\\ & + \frac{\sin\alpha}{2}|L\rangle_c\left[\cos\beta(|r|+1) - \sin\beta(|r|-1)\right]|-\rangle_t\\ & + \frac{\sin\alpha}{2}|L\rangle_c\left[\sin\beta(|r|+1) - \cos\beta(|r|-1)\right]|+\rangle_t. \end{aligned} \quad (20)$$

That is, the average fidelity of our CNOT gate can be expressed as

$$\overline{F}_{CT} = \frac{1}{4\pi^2}\int_0^{2\pi} d\alpha \int_0^{2\pi} d\beta\, |\langle\psi_{out}|\psi'_{out}\rangle|^2. \quad (21)$$

Using the same arguments for the CNOT gate, one can obtain the average fidelities of the Toffoli gate $\overline{F}_T$ and the Fredkin gate $\overline{F}_F$, shown in Fig. 5a.

Since the flying single photon may be lost during the operation for a gate, we can use $\eta = n_{output}/n_{input}$ to characterize the efficiency of a gate. Here n_{input} and n_{output} are the numbers of the input photons and the output photons, respectively. Combing the spin-selection rules in the realistic case described by Eq. (5) and the evolutions of the system from the input states to the output states, the average efficiencies of our gates, averaged over $\alpha, \beta, \delta \in [0, 2\pi]$, can be obtained as follows:

$$\overline{\eta}_{CT} = \frac{3+|r|^2}{4}, \quad (22)$$

$$\overline{\eta}_T = \frac{(3+|r|^2)(27+2|r|+4|r|^2-2|r|^3+|r|^4)}{128}, \quad (23)$$

$$\begin{aligned}\overline{\eta}_F = {} & \frac{1361-156|r|+286|r|^2+28|r|^3+239|r|^4+152|r|^5}{2048}\\ & + \frac{148|r|^6-24|r|^7-|r|^8+4|r|^9+14|r|^{10}-4|r|^{11}+|r|^{12}}{2048}. \end{aligned} \quad (24)$$

The average efficiencies of our gates vary with $g/\sqrt{\kappa\gamma}$, shown in Fig. 5b.

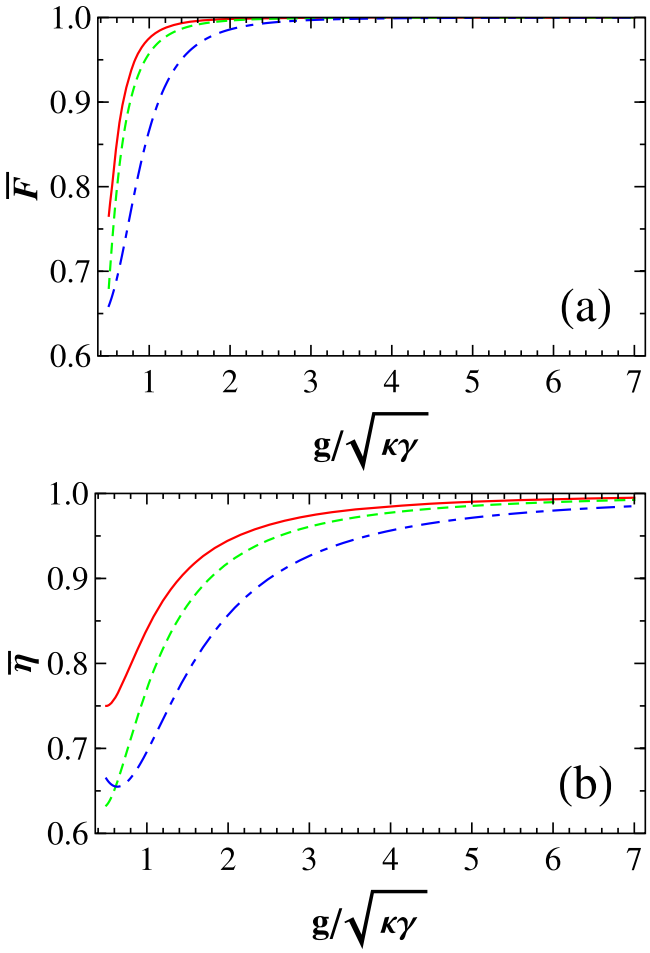

Figure 5. The average fidelities ($\overline{F}$) and the average efficiencies ($\overline{\eta}$) of our universal quantum gates on photon-NV hybrid systems vs $g/\sqrt{\kappa\gamma}$. Here the red solid line, the green dashed line, and the blue dash-dotted line correspond to those of our CNOT, Toffoli, and Fredkin gates, respectively. $g/\sqrt{\kappa\gamma} \geq 0.5$.

The feasibility of the gates. The fidelities of our gates can be reduced by the few percent by the experimental operation imperfection, such as electronic spin preparation with a low limit fidelity of $99.7 \pm 0.1\%$ to $m_s = 0$ and $99.2 \pm 0.1\%$ to $m_s = \pm 1$[26]. Bernien *et al.*[37] showed that the fidelity of their setup can be reduced by the microwave pulse errors (~3.5%), off-resonant excitation errors (~1%), spin decoherence (<1%), the charge fluctuation due to the optical frequencies, and spin-flip errors in the excited states during the optical excitation (~1%). Togan *et al.*[39] pointed out that the fidelity can be reduced by the imperfect optical transitions due to the moderate and high strain, the path length fluctuation (~4%), and the signal to noise ratio in the ZPL channel (~11%). The charge fluctuation and the imperfect electron-spin population can be decreased by exploiting a repeated-until-success (the negative charge state and on resonance) fashion[37] before performing our gates.

References

1. Nielsen, M. A. & Chuang, I. L. *Quantum Computation and Quantum Information* (Cambridge University, Cambridge, 2000).
2. Barenco, A. *et al.* Elementary gates for quantum computation. *Phys. Rev. A* **52,** 3457–3467 (1995).
3. Liu, Y., Long, G. L. & Sun, Y. Analytic one-bit and CNOT gate constructions of general n-qubit controlled gates. *Int. J. Quant. Inf.* **06,** 447–462 (2008).
4. Vatan, F. & Williams, C. Optimal quantum circuits for general two-qubit gates. *Phys. Rev. A* **69,** 032315 (2004).
5. Shende, V. V., Markov, I. L. & Bullock, S. S. Minimal universal two-qubit controlled-NOT-based circuits. *Phys. Rev. A* **69,** 062321 (2004).
6. Feng, G. R., Xu, G. F. & Long, G. L. Experimental realization of nonadiabatic holonomic quantum computation. *Phys. Rev. Lett.* **110,** 190501 (2013).
7. Xu, G. & Long, G. Universal nonadiabatic geometric gates in two-qubit decoherence-free subspaces. *Sci. Rep.* **4,** 6814 (2014).
8. Xu, G. & Long, G. Protecting geometric gates by dynamical decoupling. *Phys. Rev. A* **90,** 022323 (2014).
9. Heilmann, H., Gräfe, M., Nolte, S. & Szameit, A. A novel integrated quantum circuit for high-order W-state generation and its highly precise characterization. *Sci. Bull.* **60,** 96–100 (2015).
10. Xu, J. S. & Li, C. F. Quantum integrated circuit: Classical characterization. *Sci. Bull.* **60,** 141–141 (2015).
11. Ren, B. C., Wei, H. R. & Deng, F. G. Deterministic photonic spatial-polarization hyper-controlled-not gate assisted by a quantum dot inside a one-side optical microcavity. *Laser Phys. Lett.* **10,** 095202 (2013).

12. Ren, B. C. & Deng, F. G. Hyper-parallel photonic quantum computation with coupled quantum dots. *Sci. Rep*. **4,** 4623 (2014).
13. Ren, B. C., Wang, G. Y. & Deng, F. G. Universal hyperparallel hybrid photonic quantum gates with dipole-induced transparency in the weak-coupling regime. *Phys. Rev. A* **91,** 032328 (2015).
14. Shi, Y. Y. Both Toffoli and controlled-not need little help to do universal quantum computation. *Quant. Inf. Comput.* **3,** 084–092 (2003).
15. Fredkin, E. & Toffoli, T. Conservative logic. *Int. J. Theor. Phys.* **21,** 219–253 (1982).
16. Shende, V. V. & Markov, I. L. On the CNOT-cost of Toffoli gate. *Quant. Inf. Comput.* **9,** 461–468 (2009).
17. Smolin, J. A. & DiVincenzo, D. P. Five two-bit quantum gates are sufficient to implement the quantum Fredkin gate. *Phys. Rev. A* **53,** 2855–2856 (1996).
18. Zhang, C., Li, C. F. & Guo, G. C. Experimental demonstration of photonic quantum ratchet. *Sci. Bull.* **60,** 249–255 (2015).
19. Long, G. L. & Zhang, T. C. Quantum ratchet with photons. *Sci. Bull.* **60,** 278 (2015).
20. Balasubramanian, G. *et al.* Ultralong spin coherence time in isotopically engineered diamond. *Nat. Mater.* **8,** 383–387 (2009).
21. Jelezko, F., Gaebel, T., Popa, I., Gruber, A. & Wrachtrup, J. Observation of coherent oscillations in a single electron spin. *Phys. Rev. Lett.* **92,** 076401 (2004).
22. Gaebel, T. *et al.* Room-temperature coherent coupling of single spins in diamond. *Nat. Phys.* **2,** 408–413 (2006).
23. Fuchs, G. D., Dobrovitski, V. V., Toyli, D. M., Heremans, F. J. & Awschalom, D. D. Gigahertz dynamics of a strongly driven single quantum spin. *Science* **326,** 1520–1522 (2009).
24. Buckley, B. B., Fuchs, G. D., Bassett, L. C. & Awschalom, D. D. Spin-light coherence for single-spin measurement and control in diamond. *Science* **330,** 1212–1215 (2010).
25. Jiang, L. *et al.* Repetitive readout of a single electronic spin via quantum logic with nuclear spin ancillae. *Science* **326,** 267–272 (2009).
26. Robledo, L. *et al.* High-fidelity projective read-out of a solid-state spin quantum register. *Nature* **477,** 574–578 (2011).
27. Dutt, M. V. G. *et al.* Quantum register based on individual electronic and nuclear spin qubits in diamond. *Science* **316,** 1312–1316 (2007).
28. Childress, L. *et al.* Coherent dynamics of coupled electron and nuclear spin qubits in diamond. *Science* **314,** 281–285 (2006).
29. Fuchs, G. D., Burkard, G., Klimov, P. V. & Awschalom, D. D. A quantum memory intrinsic to single nitrogen-vacancy centers in diamond. *Nat. Phys*. **7,** 789–793 (2011).
30. Jelezko, F. *et al.* Observation of coherent oscillation of a single nuclear spin and realization of a two-qubit conditional quantum gate. *Phys. Rev. Lett.* **93,** 130501 (2004).
31. van der Sar, T. *et al.* Decoherence-protected quantum gates for a hybrid solid-state spin register. *Nature* **484,** 82–86 (2012).
32. Yang, W. L., Yin, Z. Q., Xu, Z. Y., Feng, M. & Du, J. F. One-step implementation of multi-qubit conditional phase gating with nitrogen-vacancy centers coupled to a high-*Q* silica microsphere cavity. *Appl. Phys. Lett*. **96,** 241113 (2010).
33. Wei, H. R. & Deng, F. G. Compact quantum gates on electron-spin qubits assisted by diamond nitrogen-vacancy centers inside cavities. *Phys. Rev. A* **88,** 042323 (2013).
34. Wang, C., Zhang, Y., Jiao, R. Z. & Jin, G. S. Universal quantum controlled phase gates on photonic qubits based on nitrogen vacancy centers and microcavity resonators. *Opt. Express* **21,** 19252–19260 (2013).
35. Neumann, P. *et al.* Multipartite entanglement among single spins in diamond. *Science* **320,** 1326–1329 (2008).
36. Xu, Z. Y., Hu, Y. M., Yang, W. L., Feng, M. & Du, J. F. Deterministically entangling distant nitrogen-vacancy centers by a nanomechanical cantilever. *Phys. Rev. A* **80,** 022335 (2009).
37. Bernien, H. *et al.* Heralded entanglement between solid-state qubits separated by three metres. *Nature* **497,** 86–90 (2013).
38. Pfaff, W. *et al.* Demonstration of entanglement-by-measurement of solid state qubits. *Nat. Phys*. **9,** 29–33 (2013).
39. Togan, E. *et al.* Quantum entanglement between an optical photon and a solid-state spin qubit. *Nature* **466,** 730–734 (2010).
40. Yang, W. L., Xu, Z. Y., Feng, M. & Du, J. F. Entanglement of separate nitrogen-vacancy centers coupled to a whispering-gallery mode cavity. *New J. Phys.* **12,** 113039 (2010).
41. Chen, Q., Yang, W. L., Feng, M. & Du, J. F. Entangling separate nitrogen-vacancy centers in a scalable fashion via coupling to microtoroidal resonators. *Phys. Rev. A* **83,** 054305 (2011).
42. Zhang, D., Li, J. H. & Yang, X. X. Laser-polarization-dependent spontaneous emission of the zero phonon line from single nitrogen-vacancy center in diamond. *Chin. Phys. B* **23,** 044204 (2014).
43. Chang, Y. C. *et al.* Band-selective shaped pulse for high fidelity quantum control in diamond. *Appl. Phys. Lett.* **104,** 262403 (2014).
44. Chen, X. *et al.* Subdiffraction optical manipulation of the charge state of nitrogen vacancy center in diamond. *Light: Sci. & Appl.* **4,** e230; doi: 10.1038/lsa.2015.3 (2015).
45. Pfaff, W. *et al.* Unconditional quantum teleportation between distant solid-state quantum bits. *Science* **345,** 532–535 (2014).
46. Ren, B. C. & Deng, F. G. Hyperentanglement purification and concentration assisted by diamond NV centers inside photonic crystal cavities. *Laser Phys. Lett.* **10,** 115201 (2013).
47. Wang, C., He, L., Zhang, L. Y., Zhang, Y., Ma, H. & Zhang, R. Complete entanglement analysis on electron spins using quantum dot and microcavity coupled system. *Sci. China-Phys. Mech. Astron*. **56,** 2054–2058 (2013).
48. Sheng, Y. B., Liu, J., Zhao, S. Y. & Zhou, L. Multipartite entanglement concentration for nitrogen-vacancy center and microtoroidal resonator system. *Chin. Sci. Bull.* **59,** 3507–3513 (2013).
49. Hu, C. Y., Young, A., O'Brien, J. L., Munro, W. J. & Rarity, J. G. Giant optical Faraday rotation induced by a single-electron spin in a quantum dot: Applications to entangling remote spins via a single photon. *Phys. Rev. B* **78,** 085307 (2008).
50. Hu, C. Y., Munro, W. J., O'Brien, J. L. & Rarity, J. G. Proposed entanglement beam splitter using a quantum-dot spin in a double-sided optical microcavity. *Phys. Rev. B* **80,** 205326 (2009).
51. Bonato, C. *et al.* CNOT and Bell-state analysis in the weak-coupling cavity QED regime. *Phys. Rev. Lett.* **104,** 160503 (2010).
52. Duan, L. M. & Kimble, H. J. Scalable photonic quantum computation through cavity-assisted interactions. *Phys. Rev. Lett.* **92,** 127902 (2004).
53. Wei, H. R. & Deng, F. G. Scalable photonic quantum computing assisted by quantum-dot spin in double-sided optical microcavity. *Opt. Express* **21,** 17671–17685 (2013).
54. Hua, M., Tao, M. J. & Deng, F. G. Universal quantum gates on microwave photons assisted by circuit quantum electrodynamics. *Phys. Rev. A* **90,** 012328 (2014).
55. Hua, M., Tao, M. J. & Deng, F. G. Fast universal quantum gates on microwave photons with all-resonance operations in circuit QED. *Sci. Rep*. **5,** 9274 (2015).
56. Chen, Q. & Feng, M. Quantum gating on neutral atoms in low-*Q* cavities by a single-photon input-output process. *Phys. Rev. A* **79,** 064304 (2009).
57. Wei, H. R. & Deng, F. G. Universal quantum gates on electron-spin qubits with quantum dots inside single-side optical microcavities. *Opt. Express* **22,** 593–607 (2014).
58. Manson, N. B., Harrison, J. P. & Sellars, M. J. Nitrogen-vacancy center in diamond: Model of the electronic structure and associated dynamics. *Phys. Rev. B* **74,** 104303 (2006).

59. Batalov, A. *et al.* Low temperature studies of the excited-state structure of negatively charged nitrogen-vacancy color centers in diamond. *Phys. Rev. Lett.* **102,** 195506 (2009).
60. Tamarat, P. *et al.* Spin-flip and spin-conserving optical transitions of the nitrogen-vacancy centre in diamond. *New J. Phys.* **10,** 045004 (2008).
61. Sipahigil, A. *et al.* Quantum interference of single photons from remote nitrogen-vacancy centers in diamond. *Phys. Rev. Lett.* **108,** 143601 (2012).
62. Tamarat, P. *et al.* Stark shift control of single optical centers in diamond. *Phys. Rev. Lett.* **97,** 083002 (2006).
63. Maze, J. R. *et al.* Properties of nitrogen-vacancy centers in diamond: The group theoretic approach. *New J. Phys.* **13,** 025025 (2011).
64. Bassett, L. C., Heremans, F. J., Yale, C. G., Buckley, B. B. & Awschalom, D. D. Electrical tuning of single nitrogen-vacancy center optical transitions enhanced by photoinduced fields. *Phys. Rev. Lett.* **107,** 266403 (2011).
65. Kosaka, H. & Niikura, N. Entangled absorption of a single photon with a single spin in diamond. *Phys. Rev. Lett.* **114,** 053603 (2015).
66. Walls, D. F. & Milburn, G. J. *Quantum Optics* (Springer-Verlag, Berlin, 1994).
67. An, J. H., Feng, M. & Oh, C. H. Quantum-information processing with a single photon by an input-output process with respect to low-*Q* cavities. *Phys. Rev. A* **79,** 032303 (2009).
68. Park, Y. S., Cook, A. K. & Wang, H. Cavity QED with diamond nanocrystals and silica microspheres. *Nano Lett.* **6,** 2075–2079 (2006).
69. Larsson, M., Dinyari, K. N. & Wang, H. Composite optical microcavity of diamond nanopillar and silica microsphere. *Nano Lett.* **9,** 1447–1450 (2009).
70. Barbour, R. J., Dinyari, K. N. & Wang, H. A composite microcavity of diamond nanopillar and deformed silica microsphere with enhanced evanescent decay length. *Opt. Express* **18,** 18968–18974 (2010).
71. Schietinger, S., Schröder, T. & Benson, O. One-by-one coupling of single defect centers in nanodiamonds to high-*Q* modes of an optical microresonator. Nano Lett. **8,** 3911–3915 (2008).
72. Barclay, P. E., Fu, K. M. C., Santori, C. & Beausoleil, R. G. Chip-based microcavities coupled to nitrogen-vacancy centers in single crystal diamond. *Appl. Phys. Lett.* **95,** 191115 (2009).
73. McCutcheon, M. W. & Lončar, M. Design of a silicon nitride photonic crystal nanocavity with a quality factor of one million for coupling to a diamond nanocrystal. *Opt. Express* **16,** 19136–19145 (2008).
74. Wolters, J. *et al.* Enhancement of the zero phonon line emission from a single nitrogen vacancy center in a nanodiamond via coupling to a photonic crystal cavity. *Appl. Phys. Lett.* **97,** 141108 (2010).
75. Englund, D. *et al.* Deterministic coupling of a single nitrogen vacancy center to a photonic crystal cavity. *Nano Lett.* **10,** 3922–3926 (2010).
76. Faraon, A., Barclay, P. E., Santori, C., Fu, K. M. C. & Beausoleil, R. G. Resonant enhancement of the zero-phonon emission from a colour centre in a diamond cavity. *Nat. Photon.* **5,** 301–305 (2011).
77. Gregor, M., Henze, R., Schröder, T. & Benson, O. On-demand positioning of a preselected quantum emitter on a fiber-coupled toroidal microresonator. *Appl. Phys. Lett.* **95,** 153110 (2009).
78. Albrecht, R., Bommer, A., Deutsch, C., Reichel, J. & Becher, C. Coupling of a single nitrogen-vacancy center in diamond to a fiber-based microcavity. *Phys. Rev. Lett.* **110,** 243602 (2013).
79. Teissier, J., Barfuss, A., Appel, P., Neu, E. & Maletinsky, P. Strain coupling of a nitrogen-vacancy center spin to diamond mechanical oscillator. *Phys. Rev. Lett.* **113,** 020503 (2014).
80. Barclay, P. E., Fu, K. M., Santori, C. & Beausoleil, R. G. Hybrid photonic crystal cavity and waveguide for coupling to diamond NV-centers. *Opt. Express* **17,** 9588–9601 (2009).
81. Shen, J. T. & Fan, S. Quantum critical coupling conditions for zero single-photon transmission through a coupled atom-resonator-waveguide system. *Phys. Rev. A* **82,** 021802 (2010).
82. Peng, B. *et al.* Parity-time-symmetric whispering-gallery microcavities. *Nat. Phys.* **10,** 394–398 (2014).
83. Luxmoore, I. J. *et al.* Restoring mode degeneracy in H1 photonic crystal cavities by uniaxial strain tuning. *Appl. Phys. Lett.* **100,** 121116 (2012).
84. Hagemeier, J. *et al.* H1 photonic crystal cavities for hybrid quantum information protocols. *Opt. Express* **20,** 24714–24726 (2012).
85. Bonato, C. *et al.* Tuning micropillar cavity birefringence by laser induced surface defects. *Appl. Phys. Lett.* **95,** 251104 (2009).
86. Gudat, J. *et al.* Permanent tuning of quantum dot transitions to degenerate microcavity resonances. *Appl. Phys. Lett.* **98,** 121111 (2011).
87. Bonato, C. *et al.* Strain tuning of quantum dot optical transitions via laser-induced surface defects. *Phys. Rev. B* **84,** 075306 (2011).
88. Barclay, P. E., Fu, K. M., Santori, C., Faraon, A. & Beausoleil, R. G. Hybrid nanocavity resonant enhancement of color center emission in diamond. *Phys. Rev. X* **1,** 011007 (2011).
89. Faraon, A., Santori, C., Huang, Z., Acosta, V. M. & Beausoleil, R. G. Coupling of nitrogen-vacancy centers to photonic crystal cavities in monocrystalline diamond. *Phys. Rev. Lett.* **109,** 033604 (2012).
90. Bernien, H. *et al.* Two-photon quantum interference from separate nitrogen vacancy centers in diamond. *Phys. Rev. Lett.* **108,** 043604 (2012).
91. Acosta, V. M. *et al.* Dynamic stabilization of the optical resonances of single nitrogen-vacancy centers in diamond. *Phys. Rev. Lett.* **108,** 206401 (2012).
92. Chu, Y. *et al.* Coherent optical transitions in implanted nitrogen vacancy centers. *Nano Lett.* **14,** 1982–1986 (2014).
93. Dréau, A., Spinicelli, P., Maze, J. R., Roch, J. F. & Jacques, V. Single-shot readout of multiple nuclear spin qubits in diamond under ambient conditions. *Phys. Rev. Lett.* **110,** 060502 (2013).
94. Beenakker, C. W. J., DiVincenzo, D. P., Emary, C. & Kindermann, M. Charge detection enables free-electron quantum computation. *Phys. Rev. Lett.* **93,** 020501 (2004).
95. Nemoto, K. & Munro, W. J. Nearly deterministic linear optical controlled-NOT gate. *Phys. Rev. Lett.* **93,** 250502 (2004).
96. Lin, Q. & He, B. Single-photon logic gates using minimal resources. *Phys. Rev. A* **80,** 042310 (2009).

Acknowledgements

This work was supported by the National Natural Science Foundation of China under Grant Nos 11175094 and 91221205, the National Basic Research Program of China under Grants No. 2009CB929402 and No. 2011CB9216002, and the China Postdoctoral Science Foundation under Grant No. 2014M550703. GLL is a member of the Center of Atomic and Molecular Nanosciences, Tsinghua University.

Author Contributions

H.R. and G.L. contributed equally to this work, they wrote the manuscript text, and prepared Figures 1–5. G.L. supervised the whole project.

Additional Information

Competing financial interests: The authors declare no competing financial interests.

How to cite this article: Wei, H.-R. and Lu Long, G. Hybrid quantum gates between flying photon and diamond nitrogen-vacancy centers assisted by optical microcavities. *Sci. Rep.* **5**, 12918; doi: 10.1038/srep12918 (2015).